One- and Two-Triplon Spectra of a Cuprate Ladder

S. Notbohm[1,2], P. Ribeiro[3], B. Lake[1,4], D.A. Tennant[1,4], K.P. Schmidt[5], G.S. Uhrig[6], C. Hess[3], R. Klingeler[3], G. Behr[3], B. Büchner[3], M. Reehuis[1], R.I. Bewley[7], C.D. Frost[7], P. Manuel[7], and R.S. Eccleston[8]

[1] *Hahn-Meitner-Institut Berlin, Glienicker Straße 100, 14109 Berlin, Germany*
[2] *School of Physics and Astronomy, University of St. Andrews, St. Andrews, Fife, KY16 9SS, U.K.*
[3] *Leibniz-Institut for Solid State and Material Research, IFW-Dresden, 01171, Germany*
[4] *Institut für Festkörperphysik, Technische Universität Berlin, Hardenbergstr. 36, 10623 Berlin, Germany*
[5] *Institute of Theorectical Physics, École Polytechnique Fédérale de Lausanne, 1015 Lausanne, Switzerland*
[6] *Lehrstuhl für Theoretische Physik I, Universität Dortmund, 44221 Dortmund, Germany*
[7] *ISIS Facility, Rutherford Appleton Laboratory, Chilton, Didcot OX11 OQX, U.K.*
[8] *Materials and Engineering Research Institute, Sheffield Hallam University, Howard Street, Sheffield, S1 1WB, U.K.*

(Dated: February 6, 2008)

We have performed inelastic neutron scattering on the near ideal spin-ladder compound $La_4Sr_{10}Cu_{24}O_{41}$, which will serve as a model system for the investigation of doped ladders. A key feature in the analysis was the separation of one-triplon and two-triplon scattering contributions due to an antiphase rung modulation. This enabled extraction of the one-triplon dispersion which has a spin gap of 26.4±0.3 meV, and for the first time two-triplon scattering is clearly observed. The exchange constants are determined by fitting the data to be J_{leg}=186 meV and J_{rung}=124 meV along the leg and the rung respectively. In addition to the surprisingly large difference between J_{leg} and J_{rung} a substantial ring exchange of J_{cyc}=31 meV was confirmed.

PACS numbers: 78.70.Nx 75.30.Ds 75.10.Jm 75.30.Et

The two-leg ladder, consisting of two spin-1/2 chains coupled by a Heisenberg interaction, can be thought of as a strip, two sites wide, cut out of a 2D square lattice antiferromagnet. The immediate effect of coupling the chains is to confine pairs of spin-1/2 spinons, and to generate a gapped spin singlet ground state. Short ranged singlet spin pairings on the rungs $1/\sqrt{2}\{|\uparrow\downarrow\rangle - |\downarrow\uparrow\rangle\}$ dominate the ground state, and in an inelastic neutron scattering measurement a triplet of well-defined spin-1 magnons, known as triplon [1] excitations, rather than a spinon pair continuum will appear. Further, strong higher-order ground state fluctuations should be manifest as multi-triplon continua. The spin pairings are particularly important as they provide a mechanism for the formation of charged hole pairs when doped, giving rise to condensed charge density wave or superconducting states [2, 3, 4, 5, 6]. Cuprate spin ladders share many features of the 2D high-T_c materials (pseudo-gap, non-Fermi liquid behavior) [7, 8, 9], and have similar coupling parameters. Their excitation spectra extend to several hundred meV and the development of time-of-flight spectroscopy at spallation neutron sources allows access to the full spectra resolved in wave-vector and energy for the first time. Motivated by this, we have measured the one- and two-triplon spectra of a cuprate ladder in a Mott-Hubbard insulating (MHI) phase - $La_4Sr_{10}Cu_{24}O_{41}$- using inelastic neutron scattering (INS). A full description of the dynamics is achieved using the continuous unitary transformation (CUT) method. Electrostatic environments of the oxygen tunneling result in strongly dissimilar rung and leg exchanges, and this combined with a substantial cyclic charge fluctuations render the magnetic state of the system near quantum critical (gapless).

The geometry of cuprate ladders in $La_4Sr_{10}Cu_{24}O_{41}$ is depicted in the upper part of Fig. 1. Strong antiferromagnetic super-exchange occurs through the 180° Cu-O-Cu bonds with very weak exchange between ladders via the 90° bonds. An approximate electronic Hamiltonian for the cuprates is the one-band Hubbard model

$$H = -\sum_{\langle i,j\rangle\sigma=\uparrow,\downarrow} t_{i,j}\,(c^{+}_{i,\sigma}c_{j,\sigma} + H.c.) + U\sum_{i} n_{i,\uparrow}n_{i,\downarrow} \quad (1)$$

with on-site Coulomb energy $U \sim 3.5$ eV, inter-site hopping between nearest neighbor pairs of $t \sim 0.3$ eV, and $\kappa \equiv t/U \sim \frac{1}{12}$ [10]. Charge fluctuations such as cyclic hopping processes, (suppressed in the $\kappa \to 0$ limit), are reflected in modifications to the Heisenberg spin Hamiltonian with the cyclic hopping contributing a four spin interaction term. In fact computations in the more realistic 3-band Hubbard model [11] (which include O2p and Cu3d orbitals) indicate only short range Heisenberg and four spin interactions are important with diagonal coupling across the CuO square plaquette and further neighbor interactions negligible. The resulting spin Hamiltonian is

$$H = J_{rung}\sum_{i}\mathbf{S}_{i,1}\cdot\mathbf{S}_{i,2} + J_{leg}\sum_{i,\tau}\mathbf{S}_{i,\tau}\cdot\mathbf{S}_{i+1,\tau} + H_{cyc} \quad (2)$$

$$H_{cyc} = J_{cyc}\sum_{plaquettes}[\,(\mathbf{S}_{i,1}\cdot\mathbf{S}_{i+1,1})(\mathbf{S}_{i,2}\cdot\mathbf{S}_{i+1,2}) + (\mathbf{S}_{i,1}\cdot\mathbf{S}_{i,2})(\mathbf{S}_{i+1,1}\cdot\mathbf{S}_{i+1,2}) - (\mathbf{S}_{i,1}\cdot\mathbf{S}_{i+1,2})(\mathbf{S}_{i+1,1}\cdot\mathbf{S}_{i,2})],$$

The anticipated dispersion relation for the spin-1 triplon states is plotted in the lower part of Fig. 1. For the ladder the relative ratios of the gaps at wave-vectors along the leg direction $Q_c = 0$, 0.25, 0.5 (in units of $\pi/2c$) are modified substantially by the strength of J_{cyc}.

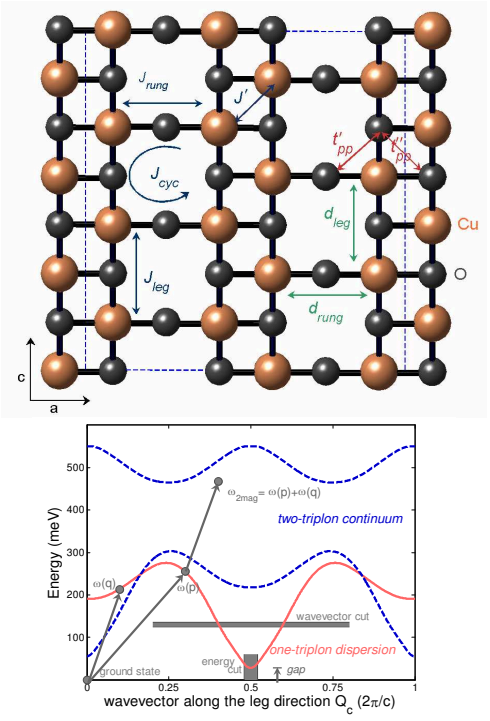

FIG. 1: (Color online) Upper part: Arrangement of the ladder planes in $La_4Sr_{10}Cu_{24}O_{41}$. Big spheres represent the copper ions, small spheres oxygen atoms. The dashed rectangle displays the unit cell in the (010) crystallographic plane for the a axis and half of the unit cell in the c axis. Lower part: S=1 excitation spectrum. There is a gap from the S=0 ground state to the S=1 triplon band (red solid curve). The two-triplon continuum states bounded by the two blue dashed curves can be constructed via the scattering of the two triplons illustrated by the arrows. A typical wave-vector cut (horizontal) and energy cut (vertical) are indicated.

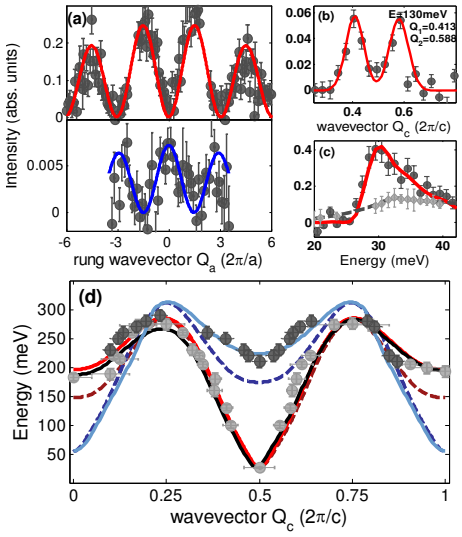

FIG. 2: (Color) (a) Cut along the rung wave-vector shows the intensity modulation Upper part: for energy of 30±5 meV and leg wave-vector of 0.45±0.05 in the rung direction for the one-triplon scattering. Lower part: for energy of 300±10 meV and leg wave-vector of 0.25 ± 0.05 for two-triplon. Solid line described in text. (b) Typical wave-vector cut through one-triplon along Q_c for energy of 130 ± 5 meV. The solid line is a Gaussian fit to extract peak position. (c) Energy cut for $0.48 < Q_c < 0.52$ to determine the energy gap. Light grey points are the corresponding cut for a hole-doped ladder. (d) Experimental points from neutron data. Theoretical one-triplon dispersion curves shown in solid red and black. Black curve includes interladder coupling. Theoretical lower boundary of one-triplon scattering shown in solid blue. Dashed lines show respective scattering without cyclic exchange.

Also shown are the boundaries of the two-triplon continuum. The intensity of the two-triplon spectrum, wave-vector and energy distribution is strongly dependent on the triplon interactions and exact composition of the ground state. Importantly, a bound spin-1 state is predicted below the two-triplon continuum. The four spin exchange term frustrates the formation of this bound mode lowering the binding energy and for coupling strengths of order $x_{cyc} = J_{cyc}/J_{rung} \sim 0.25$ will disrupt binding completely.

A remarkable property of the ladder geometry is that the sectors with even and odd triplon number do not mix because of different parity w.r.t. reflection about the centerline of the ladder. Hence even and odd contributions can be Fourier decomposed by the rung coupling, and the neutron scattering matrix elements can be expressed as a product of a neutron structure factor (NSF) dependent only on the wave-vector along the leg direction q_c, multiplied by a rung wave-vector q_a modulation. The one- and two-triplon spectra are in anti-phase with rung modulations $(1-\cos(q.a))$ and $(1+\cos(q.a))$ respectively [12], and this can be used to separate them in a neutron scattering experiment.

Here we investigate $La_4Sr_{10}Cu_{24}O_{41}$: Although intrinsically hole-doped, X-ray absorption spectroscopy reveals that in $La_x(Sr,Ca)_{14-x}Cu_{24}O_{41}$ with , residual holes are located in the more electronegative chains [13], leaving ladders undoped [14, 15]. No triplon-hole scattering is observed in the heat conductivity [16, 17].

Large $La_4Sr_{10}Cu_{24}O_{41}$ single crystals were prepared using the 'Travelling Solvent Floating Zone'-method at 9 bar oxygen pressure. Inelastic neutron scattering measurements were performed using the MAPS spectrometer at ISIS, Rutherford Appleton Laboratory, U.K. Three crystals of total mass 23 g were co-aligned with resulting mosaic spread of 0.4° in the b-c plane and 5.5° on the a-c plane. The samples were mounted with the (0kl) reciprocal lattice plane horizontal, and the c axis (leg direction) perpendicular to the incident neutron wave-vector k_i in a cryostat giving a measurement temperature of 10 K. The wave-vectors are labeled Q_c along the leg and Q_a along the rung. The magnetic cross-section was normalized using incoherent nuclear scattering from a vana-

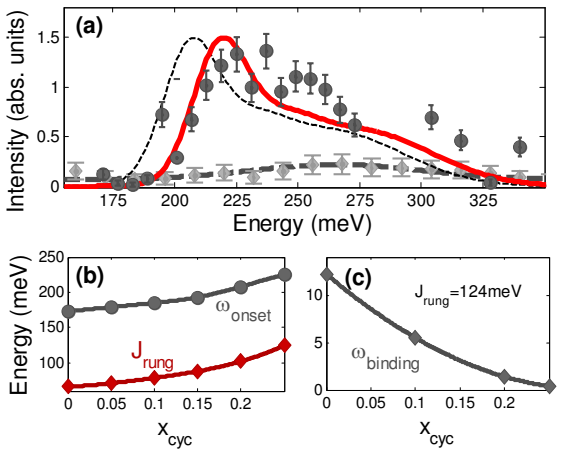

FIG. 3: (Color online) (a) Energy cut for two-triplon at $Q_c = 0.5 \pm 0.1$. Solid line is two-triplon model. Intensities had to be increased by 15 % to match data. Light grey points are the corresponding cut for a hole-doped ladder. Thin dashed line is the effect of absent cyclic exchange for fixed J_{rung}. (b) Relationship of ω_{onset} and J_{rung} w.r.t. x_{cyc}. For an onset energy of 225 meV $J_{rung} = 124$ meV and $x_{cyc} = 0.25$ are needed (see text). $J_{cyc} = x_{cyc} J_{rung}$. (c) Frustration of bound mode with increasing cyclic exchange. $\omega_{binding}$ difference between ω_{onset} and energy of bound mode.

dium standard. Data were collected for incident energies $E_i = 75.55, 363.7$ and 606.2 meV. The energy runs were monochromated using a Fermi chopper at 300 Hz for the low energy run and at 600 Hz for the other runs.

Contributions mainly from one-triplon or two-triplon scattering were separated using the antiphase rung modulation. The measured modulation is shown in Fig. 2 (a) with the one-triplon modulation fitted to $(1 - \cos(q \cdot a))$ and the two-triplon modulation to $(1 + \cos(q \cdot a))$, with corrections for the anisotropic magnetic form factor of copper [18] applied to the fitted functions. One-triplon data used in subsequent analysis was taken at the maxima between $1 < |Q_a| < 2$, see in Fig. 2 (a). For the two-triplon data, two regions of maximum two-triplon intensity $0 < |Q_a| < 0.5$ and $2.65 < |Q_a| < 3.35$ were added taking magnetic form factor corrections fully into account.

The non-magnetic background correction for the one-triplon signal was deduced via interpolation of the intensity found at energies above and below the one-triplon dispersion. The background subtracted data is displayed in Fig. 4 (a). For the two-triplon scattering, the background was deduced from the scattering observed at $Q_c = 0, 1, 2$ where the magnetic signal is expected to be weak. The result is shown in Fig. 4 (c).

The one-triplon dispersion was determined by extracting positions and intensities of measured peaks by least-squares fitting of Gaussians. A typical cut is shown in Fig. 2 (b), this gives Q_c at energy of 130 ± 5 meV indicated in Fig. 1 by the horizontal slice. These along with data points from different cuts are displayed in Fig. 2 (d). Heisenberg couplings alone are unable to account for the energy gaps of 197, 286, 26.4 meV, at wavevectors 0, 0.25, 0.5 respectively. Our computations using the CUT method [12] reveal that a substantial four-spin component $J_{cyc} = 31$ meV and Heisenberg exchange strengths along the legs $J_{leg} = 186$ meV, and rungs $J_{rung} = 124$ meV that are very different [19] are required to explain this. Computing the entire dispersion using these values (solid red line) results in excellent agreement with the data [20]. The lower boundary of the two-triplon scattering was extracted in the same manner and the data points along with the computed lower boundary of the two-triplon continuum (blue curve) are plotted in Fig. 2 (d). Also shown is the computed one-triplon (and two-triplon) dispersion in the absence of cyclic exchange (dashed curves). One can see the necessity of introduction of the cyclic exchange to describe the data within its error bars.

The CUT method is also used to compute the NSF which agrees very well with the measured scattering, see Fig. 4(b) and (d). A complete simulation of detector coverage and multicrystal mount is included with the detailed angular mosaics of each crystal, measured via neutron Laue, accounted for using a Monte Carlo integration. The uneven intensity profile of the data with wavevector is due to a combination of detector coverage and crystalline mosaic. Fig. 2(c) shows an energy cut at $Q_c = 0.5$ (vertical slice in Fig. 1, wavevector range $0.48 < |Q_c| < 0.52$). The computed NSF including instrumental corrections is shown as the red line and matches the data. Note the fitted gap is 26.4 ± 0.3 meV which is lower than found in previous measurements [21, 22].

The effect of cyclic exchange on the two triplon binding is illustrated in Fig. 3. The data points in Fig. 3 (a) show a two-triplon wave-vector cut of $Q_c = 0.5 \pm 0.1$; the red solid line is the same cut performed through the model with the determined exchange parameters. Fig. 3 (b) illustrates the dependence of the continuum onset energy ω_{onset} (measured as 224 meV), with J_{rung} determined to match the one triplon gaps at $Q_c = 0.25, 0.5$, on cyclic exchange ratio $x_{cyc} \equiv J_{cyc}/J_{rung}$. Keeping J_{rung} fixed and assuming no cyclic exchange a bound mode 12 meV below ω_{onset} would appear, shown in Fig. 3 (c) $\omega_{binding} = 12$ meV. Such a shift is indicated by the black dashed line in Fig. 3 (a) and would be detectable within our resolution limits confirming we are on the binding threshold.

Figs. 4 (c) and (d) show that nearly all the $S = 1$ two-triplon scattering weight is concentrated near the lower continuum boundary, and this is reproduced very well by calculation. Van Hove singularities in the density of states of phonon assisted IR absorption measurements indicate that $S = 0$ bound states survive as they are more stable in quantum antiferromagnets [12, 23, 24]. The CUT method also predicts the relative one and two triplon neutron scattering intensity scales. The scale factors applied to the model above are within 15% of the computations, i.e. within experimental accuracy.

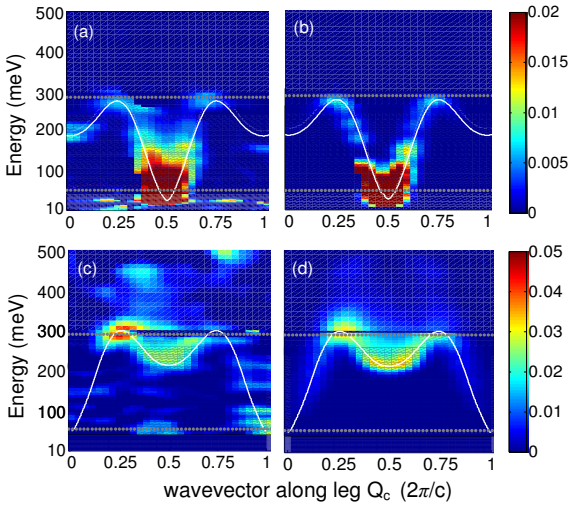

FIG. 4: (Color) (a) Measured one triplon data with nonmagnetic background subtracted. The white curve gives the theoretically calculated one triplon dispersion curve. (b) Calculated one-triplon scattering with corrections for instrumental resolution and magnetic form factor. (c) Measured two triplon data with nonmagnetic background subtracted. The white curve gives the lower boundary of the two-triplon dispersion curve. (d) Calculated two-triplon scattering.

The large difference between rung and leg exchange implies stronger hopping along the legs $t_{leg} > t_{rung}$ despite a longer pathway (d_{leg}=3.96Å, d_{rung}=3.84Å). Contributions from hopping between O2p orbitals [25] depend acutely on electrostatic environment [26]. For ladders, Fig. 1, O2p hopping along the leg, t''_{pp} is enhanced by two neighboring Cu^{2+} ions compared to the rung, t'_{pp} which has one Cu^{2+} neighbor [26] accounting for the stronger t_{leg}. Further, admixture of Cu4s states has been proposed to enhance t_{leg} hopping (by 35 %) [27, 28] compared to t_{rung}. Comparison of our values of J_{leg}, J_{rung}, and J_{cyc} with theoretical calculation should lead to a more refined model for cuprate electronic structure.

Approximate parameters for (1), $t_{leg} = 0.42$, $t_{rung} = 0.34$, $U = 3.72$ eV, follow from low order perturbation theory [29], but recourse to 3-band computations is necessary for high accuracy. To account for the CDW states shown at low temperatures in hole-doped ladders $Sr_{14-x}Ca_xCu_{24}O_{41}$ [30] electrostatic interactions $\sum_{i,a=L,R} V_{leg} n_{i,a} n_{i+1,a} + V_{rung} n_{i,L} n_{i,R}$ have been introduced in an extended Hubbard model [31]. Our MAPS measurements on the x=11.5 doped ladder ($\rho \propto T$ above $T_{CDW} \sim 80K$) which has a modest doping of 5% holes on the ladder, show the one-triplon spectra to split into multiple branches and for the gap to develop into a pseudogap (see 2(c)). Further the boundaries of the two-triplon spectra undergo dramatic changes and the lower boundary at $Q_c = 0.5$ collapses (see Fig. 3(a)). Understanding the dramatic evolution of the spin correlations from the MHI to doped metallic ladder is a challenging problem, but is necessary to bridge the gap between understanding INS from insulating quantum magnets versus strongly correlated metals such as high-T_c.

In conclusion, our high resolution INS measurements establish the full one- and two-triplon spectra in the MHI cuprate ladder, and also the accuracy of the continuous unitary transformation method. Computation of the magnetic spectra in doped ladders within the framework of an extended Hubbard model is urgently needed.

We thank T.G. Perring, H.-J. Mikeska, A.L. Läuchli, P. Schubert-Bischoff and S.-L. Drechsler for support.

[1] K.P. Schmidt *et al.*, Phys. Rev. Lett. **90**, 227204 (2003).
[2] E. Dagotto *et al.*, Phys. Rev. B **45**, 5744 (1992).
[3] T.M. Rice *et al.*, Europhys. Lett. **23**, 445 (1993).
[4] S. Gopalan, T.M. Rice, and M. Sigrist, Phys. Rev. B **49**, 8901 (1994).
[5] H. Tsunetsugu, M. Troyer, and T.M. Rice, Phys. Rev. B **51**, 16456 (1995).
[6] M. Troyer, H. Tsunetsugu, and T.M. Rice, Phys. Rev. B **53**, 251 (1996).
[7] M. Takahashi *et al.*, Physica B **237-238**, 112 (1997).
[8] E. Dagotto, Rep. Prog. Phys **62**, 1525 (1999).
[9] J.M. Tranquada *et al.*, Nature **429**, 534 (2004).
[10] K.-Y.Yang *et al.*, cond-mat\0603423.
[11] E. Müller-Hartmann and A. Reischl, Eur. Phys J. B **28**, 173 (2001)
[12] K.P. Schmidt, and G.S. Uhrig, Mod. Phys. Lett. B **19**, 1179 (2005).
[13] N. Nücker *et al.*, Phys. Rev. B **62**, 14384 (2000).
[14] S.A. Carter *et al.*, Phys. Rev. Lett. **77**, 1378 (1996).
[15] D.A. Tennant *et al.*, *unpublished.*
[16] C. Hess *et al.*, Phys. Rev. B **64**, 184305 (2001).
[17] C. Hess *et al.*, Phys. Rev. Lett. **93**, 027005 (2004).
[18] S. Shamoto *et al.*, Phys. Rev. B **48** 13817 (1993).
[19] K.P. Schmidt *et al.*, Phys. Rev. B **72**, 094419 (2005).
[20] We also explored interladder effects within the RPA. The black line in Fig. 2(b) is the dispersion computed including an interchain exchange J'=36 meV. The interladder coupling does not have a large effect on the disperion and is undetermined with experimental accuracy.
[21] R.S. Eccleston *et al.*, Phys. Rev. B **53**, R14721 (1996).
[22] M. Azuma *et al.*, Phys. Rev. Lett. **73**, 3463 (1994).
[23] M. Windt *et al.*, Phys. Rev. Lett. **87**, 127002 (2001).
[24] T. Nunner *et al.*, Phys. Rev. B **66**, 180404(R) (2002).
[25] H. Eskes, and J.H. Jefferson, Phys. Rev. B **48**, 9788 (1993).
[26] Y. Mizuno *et al.*, Phys. Rev. B **58**, R14713 (1998).
[27] M. Arai, and H. Tsunetsugu, Phys. Rev. B **56**, R4305 (1997).
[28] T.F.A Müller *et al.*, Phys. Rev. B **57** R12655 (1998).
[29] Parameters to $0(\kappa^4)$: $J_{leg} = 4t_{leg}^2/U + O(\kappa^4)$,

$J_{rung} = 4t_{rung}^2/U + O(\kappa^4)$, $J_{cyc} = 80t_{leg}^2 t_{rung}^2/U^3$; A. Rusydi *et al.*, Phys. Rev. Lett **97**, 016403 (2006).
[30] T. Nagata *et al.*, Phys. Rev. Lett. **81**, 1090 (1998).
[31] C.J. Wu, L.W. Vincent, and E. Fradkin , Phys. Rev. B **68** 115104 (2003).